Morphology effects in MgH_2 anode for lithium ion batteries

Abdel El kharbachi[a], Hanne F. Andersen[a], Magnus H. Sørby[a], Per Erik Vullum[b], Jan Petter Mæhlen[a], Bjørn C. Hauback[a]

[a] Institute for Energy Technology, P.O. Box 40, NO-2027 Kjeller, Norway

[b] SINTEF Materials and Chemistry, P.O. Box 4760 Sluppen, NO-7465 Trondheim, Norway

Abstract

In order to acquire reproducible electrodes relevant for Li ion batteries new MgH_2 electrodes are successfully obtained from homogenous slurries in *N*-Methyl-2-Pyrrolidone "NMP" solvent. The electrodes are aimed to elucidate the contribution of the cell components to the electrochemical cycling, in terms of morphology and composition. Various electrode preparations were tested and compared regarding their interaction with Li in a half-cell. The obtained electrochemical cycling curves are discussed according to the ball-milling-induced structural morphology changes and presence of carbon additives, along with the effect of the kinetic rate on the conversion reaction mechanism.

Keywords: MgH_2 anode; structural morphology; carbon additive; conversion reaction; Li-ion battery

1. Introduction

Conversion-type anodes are interesting for Li-ion batteries and beyond (Na-ion, Mg and redox flow batteries) as they demonstrate superior capacities and novel chemistries which are different from the well-known intercalation systems [1-7]. MgH_2 as anode reacts with $2Li^+$ in a conversion reaction, leading to the formation of Mg and precipitation of 2LiH with a high theoretical capacity of 2037 $mAh.g^{-1}$ (compared to graphite-anode 372 $mAh.g^{-1}$) and the lowest charge-discharge polarization of any tested conversion-type material [2, 8]. These excellent properties indicate that hydride materials could be suitable for applications in the future batteries, such as electrical vehicles. However, a major challenge is the capacity loss after few cycles [8]. It has been reported a beneficial effect of mechanochemical reaction of MgH_2 with Li metal leading to a composite of Mg embedded in a LiH matrix. Starting from the lithiated state, such Mg/2LiH composite has reached a reversible capacity of 1064 $mAh.g^{-1}$ during the first cycle [9, 10]. However, the poor electronic conductivity of iono-covalent hydrides, such as MgH_2, has to be taken in consideration, in addition to the insulating character of LiH during re-charge. Commercial MgH_2 (particle size 25–100 μm) has shown poor electrochemical activity and practically no discharge capacity. However, even if the particle size is reduced to 0.1-5 μm by ball milling, the agglomeration of the particles into 5-30 μm agglomerates can limit the reversibility of the reactional process [2]. Furthermore, the addition of carbon black has been stated helpless since the charge capacity is lost after one discharge. It has also been reported, that the obtained MgH_2 crystallites are in the range of a few nanometers after one cycle [2], which can play a key role in the reduction of the length of the diffusion pathways. On the other hand, the positive volume change of the electrode during the discharge process can influence the conductivity between the particles. Based on lattice parameters, the bulk volume increase from tetra-MgH_2 to 2LiH/Mg is about 85%, such a volume excess is dominated by the presence of the LiH insulator. Thus, the electrode formulation, including shape, morphology and additives, has a large influence on the cycling performance [8, 11-13]. However no systematic study has been reported yet regarding the effect of the morphology and cycling conditions of the active material. Hence, more understanding of

the mechanistic properties of hydride-based anodes is highly desirable.

Here, we report studies of different MgH_2 anode composite materials which were tape-casted on a Cu current collector using homogenous slurries in *N*-Methyl-2-Pyrrolidone solvent. Various electrode preparations and cycling conditions were used and compared regarding their interaction with Li in a half-cell. The contribution and the nature of the morphology of the MgH_2–based electrodes before and after cycling are presented and discussed, along with some kinetic aspects of the conversion reaction.

2. Experimental

MgH_2 was purchased from Alpha-Aesar (98% purity). The MgH_2 was ball-milled under argon atmosphere for periods between 0.5 and 24 h using a Fritsch Pulverisette 6 planetary ball-mill with stainless steel vials and balls (ball-to-powder ratio 40:1, rotation speed 350 rpm). The milled MgH_2 powders were ground with carbon black for additional 1 h using Spex 8000 mixer/mill (ball-to-powder 8:1) for improved electronic conductivity. The various samples and their estimated crystallite/particle size are summarized in table 1. MgH_2 electrodes (~26µm thick) were obtained from slurries in *N*-Methyl-2-Pyrrolidone solvent (MgH_2/carbon black/Pvdf (Polyvinylidene fluoride) binder, ~7:2:1 by wt. fraction), and the homogenous suspensions were spread out on a copper foil (Cu-dendritic, Battery-grade, Schlenk) before drying over night at 120°C under dynamic vacuum. The total carbon black contained a mixture of carbon Super-P® (C_{SP}, TIMCAL), specific surface area (SSA) 75 $m^2.g^{-1}$, and mesoporous carbon (C_{meso}, Sigma-Aldrich) in the weight ratio C_{SP}/C_{meso} 1:1. Two grades of C_{meso} were tested C_{meso1} and C_{meso2}. They have the following morphological characteristics, average particle size / pore size / SSA of 45 µm / 10 nm / 200 $m^2.g^{-1}$ and 0.5 µm / 14 nm / 75 $m^2.g^{-1}$ for C_{meso1} and C_{meso2}, respectively.

All sample handling was performed in a MBrun glove box under argon atmosphere (H_2O and O_2 < 0.1 ppm). The liquid electrolyte 1M LiPF6 in 1:1 ethylene carbonate/diethylene carbonate (LP30, BASF) was used without any additional additives and showed no reaction with the hydride. A home-

made “ETH-cell” battery cell consisting of a stainless-steel outer casing and inner parts in titanium was used for cycling. The cell was loaded with the active material in the glovebox, then covered by a separator layer (Whatman®) soaked in 80 µl of the selected electrolyte, before the lithium foil was placed on top. The assembled cells were cycled in galvanostatic mode at 30°C between 0.2–2.5 V vs. Li^+/Li redox couple (C-rate C/20) using an Arbin Battery cycler (Arbin Instruments). The electrochemical capacity is reported per mass unit (g) of the MgH_2 active material. The lithiation of carbon black is expected to be small and similar for all samples [11] and its contribution was neglected. The voltage cut-off at 0.2 V was applied for all the cells so that to avoid the formation of the hcp Mg-type and bcc Li-type solid solutions at lower voltage [2, 13].

Synchrotron radiation powder X-ray diffraction (SR-PXD) patterns were obtained at the Swiss-Norwegian Beamlines (SNBL, BM01), ESRF, Grenoble with a Pilatus2M 2-dimensional detector and a wavelength of 0.777873 Å. The samples were contained in 0.5 mm boronglass capillaries that were rotated 90 degrees during the 30 second exposure. The sample-detector distance was 345.97 mm. 1D data were obtained by integration of the 2D diffraction patterns with the program Bubble [14]. Crystallite size was obtained with the Scherrer equation from the positions and FWHM (Full Width at Half Maximum) of the diffraction peaks. The broadness of the Bragg peaks was corrected for the instrumental contribution using LaB_6 standard. The microstrain contribution to the broadening was disregarded as it remains at a minimum level even after long-time milling of MgH_2 [15]. Scanning electron microscopy (SEM) was performed using a Hitachi S-4800. Focused ion beam – scanning electron microsocopy (FIB-SEM) was carried out with a FEI Helios 600 dualBeam FIB. The Ga^+ ion beam was used to cut down through the electrode for cross-section imaging. TEM was performed with a double Cs corrected JEOL coldFEG ARM200CF, operated at 200 kV.

Table 1. Samples, milling times, estimated crystallite size (XRD) and particle size range (SEM/TEM).

Designation	Milling time, h	Crystallite size, nm	Particle size, μm
As-received	0	97±18	25-100
MgH_2-A	½	18±3	<5
MgH_2-B	2½	10±2	<1
MgH_2-C	5	8±1	0.1–0.4
MgH_2-D	10	7±1	0.05–0.3
MgH_2-E	24	7±1	0.05–0.2

3. Results and Discussion

3.1. Materials characterization

Fig.1 shows the SR-PXD patterns of MgH_2 milled at different times as well as the as-received material. For the as-received powder, all Bragg peaks correspond to *tetra*-MgH_2 phase with very small amounts of Mg. By milling, it can be noticed a significant increase of the intensity of the Mg reflections and the appearance of the metastable *ortho*-MgH_2 phase after ½ h of milling. This latter phase has been shown to form in minor amounts from *tetra*-MgH_2 during milling [16-18] and under high pressure [19, 20]. Note that *tetra*-MgH_2 and *ortho*-MgH_2 have band gap energies of 5.6 and 5.3 eV respectively [21], a difference that can affect the electrical properties of the anode material. The width of the Bragg peaks increases with milling time in agreement with the obtained crystallites size which vary from 18 to 7 nm, corresponding to the ½ h and 24 h milled samples. The SR-PXD data also show the presence of minor amounts of MgO which increase slightly with milling time.

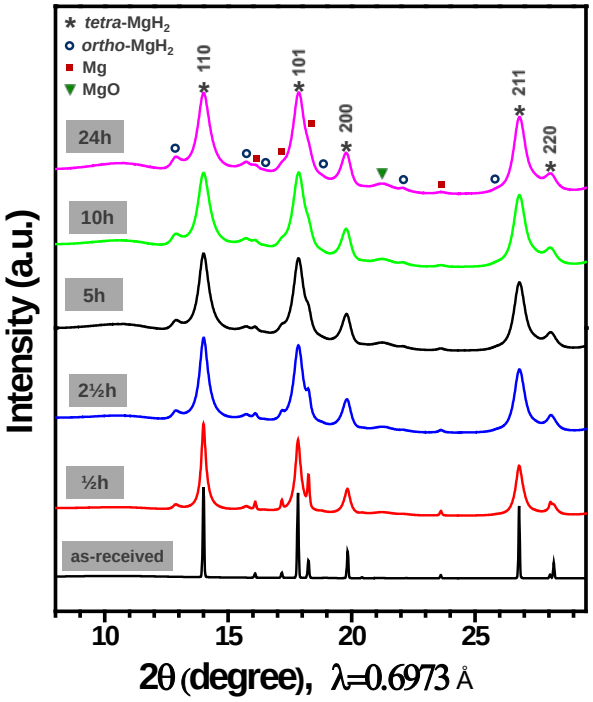

Figure 1. SR-PXD patterns of the ball-milled MgH_2 at different milling times. Muller indices (hkl) are shown for the *tetra*- MgH_2 phase.

SEM micrographs from the as-received and selected milled samples, before the addition of any battery components (carbon, binder and electrolyte) are shown in Fig.2. The flake-shaped as-received MgH_2 undergoes a drastic morphological change after ½ h milling by a particle size reduction from 25-100 µm to around 5 µm. With increasing milling time, meaning after 5 h and 10 h, a significant amount of the particles are in the sub-micron range even though a few coarse particles are still present. The particles are even smaller for the 24h-milled powder but it is difficult to estimate their size due to agglomeration.

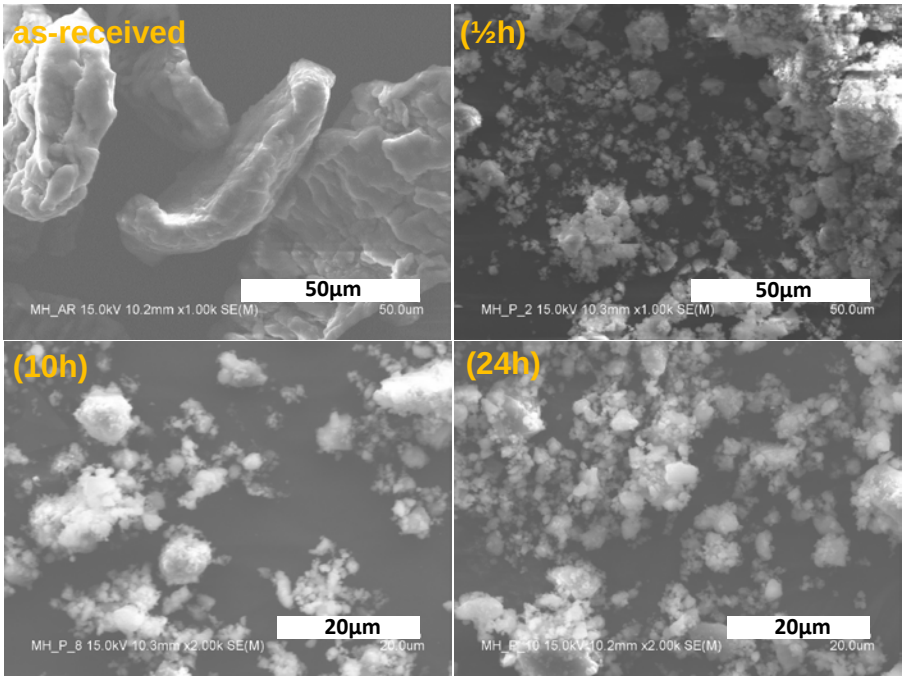

Figure 2. SEM micrographs of as-received and MgH_2 powders milled for ½, 10 and 24 h, respectively.

Bright field TEM images are shown in Fig.3 for the as-milled samples (MgH_2-C, MgH_2-D and MgH_2-E) with a better view of the distribution of particles and shape. The scattering domains are heterogeneous and follow the expected reduction trend for the particle size for the three samples. A significantly reduced particle size after 5 h milling is confirmed. With increasing milling time, i.e. after 10 h and 24 h, smaller particles in the order of 100 nm appear. Based on TEM observations, an estimation of the particle size range for these three samples is given in table 1.

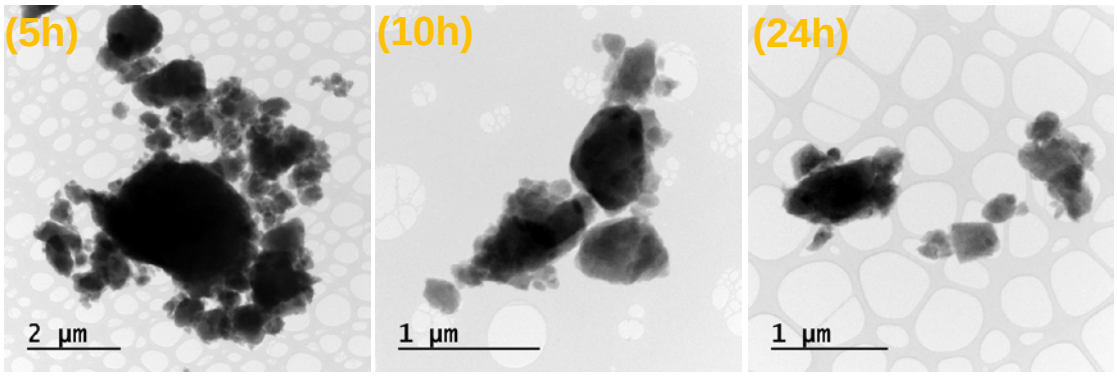

Figure 3. TEM micrographs of milled MgH_2 powders for 5, 10 and 24 h respectively.

3.2. Battery tests of MgH_2 anodes

The electrochemical cycling for the 3 first cycles of MgH_2 mixed with carbon black (C_{SP}) by hand-grinding and ball-milling, are presented in Fig. 4(a) and (b), respectively. The sample milled with carbon exhibits the highest discharge capacity, 1450 $mAh.g^{-1}$ (1.4 Li equivalent). The cycling performances are similar to the one obtained in ref. [8], but as the samples are treated in different ways that makes the comparison difficult. However, only 38% of this capacity is reversible during the first cycle. The hand grinded MgH_2 with carbon black shows a significantly smaller initial capacity, 1050 $mAh.g^{-1}$, and a much quicker capacity loss during the first 3 cycles.

In the attempt to improve the carbon black used in this study, mesoporous carbon black C_{meso} is added to the C_{SP}. Fig. 4(c) compares the effect of the addition of mesoporous carbon of two different grades (C_{meso1} and C_{meso2}) in the MgH_2–E based anode. The discharge profile shows a clear improvement when C_{meso1} is added. It comes out that the higher surface area of C_{meso1} compared to C_{meso2} plays a key role in the dispersion of carbon black for better contact and improved conductivity. The optimization of the amount of the selected C_{meso1} is shown in Fig. 4(d). The sample with 10wt.% C_{meso1} indicates higher reversible capacity and flat (dis)charge plateaus with lower overvoltage. This composition of 10 wt.% C_{meso1} is thus selected for the following samples.

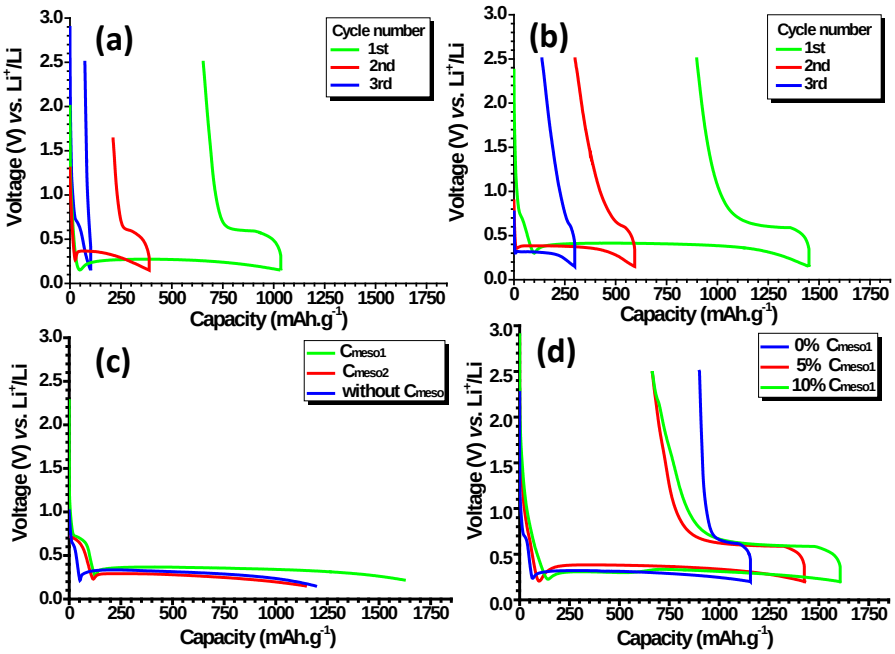

Figure 4. Effect of the mixing conditions of the MgH_2–E sample with carbon black on the discharge/charge cycling profiles (3 cycles, C/20) using (a) hand grinding and (b) ball-milling for 1h . Effect of the addition of C_{meso} (c) on the discharge profile using two different carbon grades C_{meso1} and C_{meso2} and (d) as function of the amount of C_{meso1}.

To clarify how the MgH_2 anode performances are affected by the particle size, cycling records of the samples milled at different times have been undertaken. Additional milling of the samples for 1 h with carbon black is assumed to be negligible regarding the microstructural changes.

The effect of the milling time, reflected by the different morphology samples (Table 1), is shown in Fig. 5(a). The samples show increased discharge capacity as a function of the milling time. However, peculiar trends are observed when comparing the reversible capacities. Despite the lower initial capacity, the 10h milled sample features an improved reversibility (630 $mAh.g^{-1}$) compared to the 24 h milled sample (510 $mAh.g^{-1}$). In addition, the sample milled for short time (MgH_2–C) behave (1^{st} cycle) similar to the one obtained during the 2^{nd} cycle of the corresponding MgH_2–E sample in Fig. 4(b). The kinetics of the electrochemical transformations of the samples MgH_2–C, MgH_2–D and MgH_2–E were tested at different C-rates and as function of the milling time (Fig. 5b). At a fixed rate, all the samples show an increase of the reversible capacity with decreased particle size, being

observed for all the 3 rates. On the other hand, a substantial kinetic effect is observed for samples with smaller particle size, being evidenced by larger reversible capacity increments. This interesting "apparent" increase of the reversible capacity can be connected to degradation aspects, such as SEI formation and its interactions with LiH, occurring in turns at different rate.

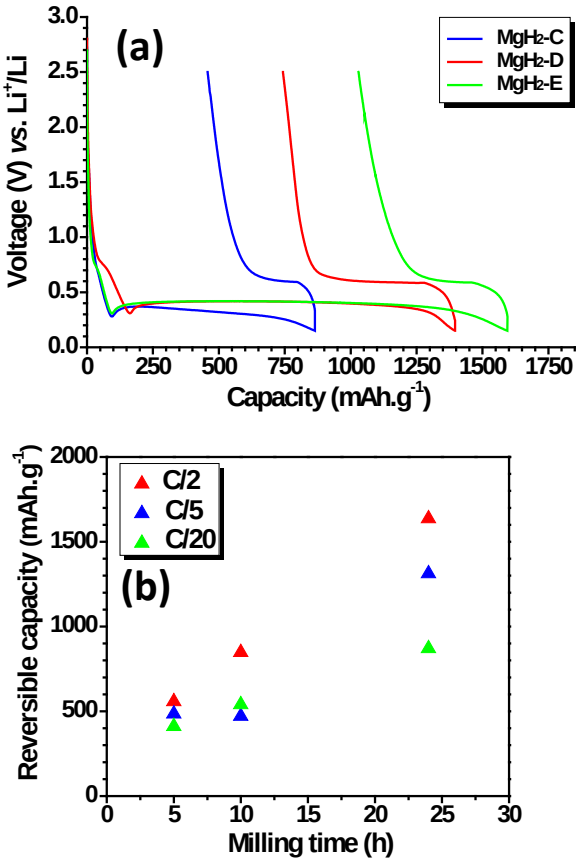

Figure 5. Comparison of the electrochemical performance of the MgH_2–C, MgH_2–D and MgH_2–E based anodes (1 cycle). (a) Effect of the particle morphology on the electrochemical cycling (C/20) according to the milling times. (b) Rate effect on the reversible capacity plotted against milling time.

The MgH_2–D sample cycled 10 times was analyzed by FIB-SEM. Fig. 6 shows the cross section secondary electron images of the eroded electrode with various agglomerates. Fig.6a displays the inner part of the composite electrode, in which contact anomalies at the anode/current collector interface can be detected. At higher magnification (Fig.6b), along the cross section, it can be seen the presence of small particles (50 nm range) embedded in a continuous porous matrix, presumably a

mixture of MgH_2 and inactive LiH/Mg composite. As a consequence, the electrode presents no further electrochemical reversibility owing to poor electronic conductivity and mechanical stability in the presence of LiH. Similar to other conversion-type anodes, an activation process of the electrode composite could take place with formation of a solid electrolyte interphase (SEI) at the surface of the carbon black and MgH_2 material, resulting from minor decomposition of the electrolyte [22].

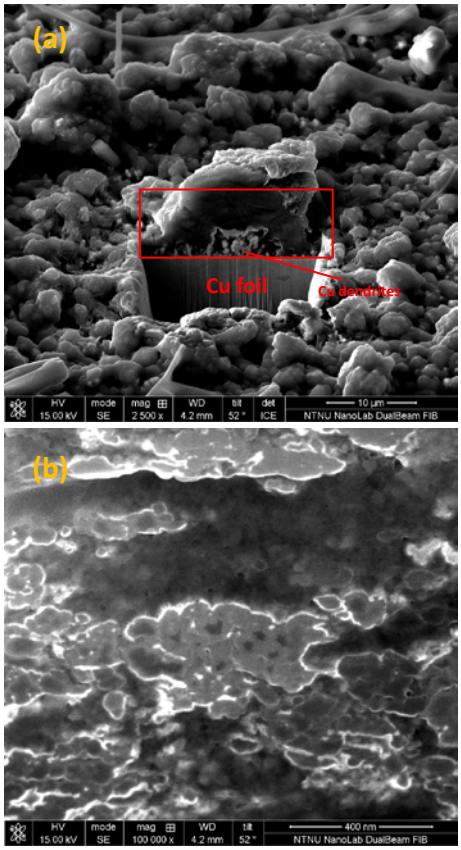

Figure 6. Secondary electron micrographs of the MgH_2–D electrode after 10 cycles. (a) Cross section obtained by FIB-SEM and (b) higher magnification image of the active part of the cross section.

4. Conclusions

Conversion-type reactions seem more dependent on the cycling conditions and the electrode formulation. New MgH_2 electrodes were successfully prepared in a slurry method and tested in different configurations. Once the ratio MgH_2/Carbon/binder optimized, the discharge capacity of the half-cell was observed to increase by decreasing the particle/crystallite size. During re-charge, significant amounts of the Mg/LiH byproducts are irreversible and therefore become inactive. Post-mortem analysis of the electrode after 10 cycles, shows nanoscopic particles (MgH_2 and inactive Mg/LiH) favoring agglomerations in a continuous porous matrix (LiH and battery residue) with possible contact loss at the carbon-LiH-Mg interfaces. The growth of a thick layer of MgH_2 on the partially active Mg/LiH composite, is may be also the factor behind the loss of the reversible capacity owing to reduced electrical contacts. The kinetic rate seems to affect the cycling performance as a function of the milling time. At fixed rate, a general trend is observed regarding the increase of the reversible capacity as function of the particle size. However, for the electrodes with the same morphology, an apparent increase of the reversible capacity upon cycling rates is observed. It can be concluded that the “failure” mechanism is reaction rate-dependent; part of it may be associated to the compatibility of the complex SEI formation regarding the highly dispersive LiH matrix. Work is in progress to confirm this abnormal kinetic model and to explore the relevance of SEI-free solid electrolyte for the same morphology anodes.

Acknowledgements

This work is financially supported by Research Council of Norway under the program EnergiX, Project no. 244054, LiMBAT - "Metal hydrides for Li-ion battery anodes". We acknowledge the skillful assistance from the staff of SNBL at ESRF, Grenoble, France.

References

[1] Poizot P, Laruelle S, Grugeon S, Dupont L, Tarascon JM. Nano-sized transition-metal oxides as negative-electrode materials for lithium-ion batteries. Nature. 2000;407:496-9.

[2] Oumellal Y, Rougier A, Nazri GA, Tarascon JM, Aymard L. Metal hydrides for lithium-ion batteries. Nat Mater. 2008;7:916-21.

[3] Larcher D, Tarascon JM. Towards greener and more sustainable batteries for electrical energy storage. Nat Chem. 2015;7:19-29.

[4] Teprovich JA, Zhang J, Colón-Mercado H, Cuevas F, Peters B, Greenway S, et al. Li-Driven Electrochemical Conversion Reaction of AlH3, LiAlH4, and NaAlH4. Journal of Physical Chemistry C. 2015;119:4666-74.

[5] Oumellal Y, Zaidi W, Bonnet JP, Cuevas F, Latroche M, Zhang J, et al. Reactivity of TiH2 hydride with lithium ion: Evidence for a new conversion mechanism. Int J Hydrogen Energy. 2012;37:7831-5.

[6] Sartori S, Cuevas F, Latroche M. Metal hydrides used as negative electrode materials for Li-ion batteries. Appl Phys A. 2016;122:135.

[7] Meggiolaro D, Farina L, Silvestri L, Panero S, Brutti S, Reale P. Lightweight Borohydrides Electro-Activity in Lithium Cells. Energies. 2016;9:238.

[8] Brutti S, Mulas G, Piciollo E, Panero S, Reale P. Magnesium hydride as a high capacity negative electrode for lithium ion batteries. J Mater Chem. 2012;22:14531-7.

[9] Oumellal Y, Rougier A, Tarascon JM, Aymard L. 2LiH + M (M = Mg, Ti): New concept of negative electrode for rechargeable lithium-ion batteries. J Power Sources. 2009;192:698-702.

[10] Hanada N, Kamura A, Suzuki H, Takai K, Ichikawa T, Kojima Y. Electrochemical charge and discharge properties for the formation of magnesium and aluminum hydrides. J Alloys Compd. 2011;509, Supplement 2:S584-S7.

[11] Oumellal Y, Zlotea C, Bastide S, Cachet-Vivier C, Leonel E, Sengmany S, et al. Bottom-up preparation of MgH2 nanoparticles with enhanced cycle life stability during electrochemical conversion in Li-ion batteries. Nanoscale. 2014;6:14459-66.

[12] Zaïdi W, Oumellal Y, Bonnet JP, Zhang J, Cuevas F, Latroche M, et al. Carboxymethylcellulose and carboxymethylcellulose-formate as binders in MgH2–carbon composites negative electrode for lithium-ion batteries. J Power Sources. 2011;196:2854-7.

[13] Aymard L, Oumellal Y, Bonnet J-P. Metal hydrides: an innovative and challenging conversion reaction anode for lithium-ion batteries. Beilstein Journal of Nanotechnology. 2015;6:1821-39.

[14] Dyadkin V, Pattison P, Dmitriev V, Chernyshov D. A new multipurpose diffractometer PILATUS@SNBL. Journal of Synchrotron Radiation. 2016;23:825-9.

[15] Varin RA, Czujko T, Wronski Z. Particle size, grain size and γ-MgH 2 effects on the desorption properties of nanocrystalline commercial magnesium hydride processed by controlled mechanical milling. Nanotechnology. 2006;17:3856.

[16] Selvam P, Viswanathan B, Swamy CS, Srinivasan V. Magnesium and magnesium alloy hydrides. Int J Hydrogen Energy. 1986;11:169-92.

[17] Schulz R, Huot J, Liang G, Boily S, Lalande G, Denis MC, et al. Recent developments in the applications of nanocrystalline materials to hydrogen technologies. Materials Science and Engineering: A. 1999;267:240-5.

[18] Yavari AR, de Castro JFR, Vaughan G, Heunen G. Structural evolution and metastable phase detection in MgH2–5%NbH nanocomposite during in-situ H-desorption in a synchrotron beam. J Alloys Compd. 2003;353:246-51.
[19] Bastide J-P, Bonnetot B, Létoffé J-M, Claudy P. Polymorphisme de l'hydrure de magnesium sous haute pression. Mater Res Bull. 1980;15:1215-24.
[20] Vajeeston P, Ravindran P, Hauback BC, Fjellvåg H, Kjekshus A, Furuseth S, et al. Structural stability and pressure-induced phase transitions in MgH2. Physical Review B. 2006;73:224102.
[21] Moysés Araújo C, Ahuja R. Electronic and optical properties of pressure induced phases of MgH2. J Alloys Compd. 2005;404–406:220-3.
[22] Mahmoud A, Chamas M, Lippens P-E. Electrochemical impedance study of the solid electrolyte interphase in MnSn2 based anode for Li-ion batteries. Electrochim Acta. 2015;184:387-91.